◆ Human Brain Mapping 35:4316–4329 (2014) ◆

Visualization of the Amygdalo–Hippocampal Border and its Structural Variability by 7T and 3T Magnetic Resonance Imaging

Johanna Derix,[1,2,3] Shan Yang,[4] Falk Lüsebrink,[4] Lukas Dominique Josef Fiederer,[1,2,3] Andreas Schulze-Bonhage,[2,3] Ad Aertsen,[1,3] Oliver Speck,[4,5,6,7] and Tonio Ball[2,3]*

[1]*Faculty of Biology, University of Freiburg, Freiburg, Germany*
[2]*Epilepsy Center, University Medical Center Freiburg, Albert-Ludwig University, Freiburg, Germany*
[3]*Bernstein Center Freiburg (BCF), Freiburg, Germany*
[4]*Department of Biomedical Magnetic Resonance, Institute for Experimental Physics, Faculty of Natural Sciences, University of Magdeburg, Magdeburg, Germany*
[5]*Leibniz Institute for Neurobiology, Magdeburg, Germany*
[6]*German Centre for Neurodegenerative Diseases (DZNE), Site Magdeburg, Germany*
[7]*Center for Behavioral Brain Sciences, Magdeburg, Germany*

Abstract: The amygdala and the hippocampus are two adjacent structures in the medial temporal lobe that have been broadly investigated in functional and structural neuroimaging due to their central importance in sensory perception, emotion, and memory. Exact demarcation of the amygdalo-hippocampal border (AHB) is, however, difficult in conventional structural imaging. Recent evidence suggests that, due to this difficulty, functional activation sites with high probability of being located in the hippocampus may erroneously be assigned to the amygdala, and vice versa. In the present study, we investigated the potential of ultra-high-field magnetic resonance imaging (MRI) in single sessions for detecting the AHB in humans. We show for the first time the detailed structure of the AHB as it can be visualized in T1-weighted 7T *in vivo* images at 0.5-mm^3 isotropic resolution. Compared to data acquired at 3T, 7T images revealed considerably more structural detail in the AHB region. Thus, we observed a striking inter-hemispheric and interindividual variability of the exact anatomical configuration of the AHB that points to the necessity of individual imaging of the AHB as a prerequisite for accurate anatomical assignment in this region. The findings of the present study demonstrate the usefulness of ultra-high-field structural MRI to resolve anatomical ambiguities of the human AHB. Highly accurate morphometric and functional investigations in this region at 7T may allow addressing such hitherto unexplored issues as whether the structural configuration of the AHB is related to functional differences in amygdalo-hippocampal interaction. *Hum Brain Mapp 35:4316–4329, 2014.*

Additional Supporting Information may be found in the online version of this article.

Contract grant sponsor: German Research Foundation (DFG); Contract grant number: Wa2673/3-1; Contract grant sponsor: DFG; Contract grant numbers: EXC 1086 BrainLinks-BrainTools to the University of Freiburg, Germany.

*Correspondence to: Tonio Ball, AG Ball, Engelbergerstr. 21, 1. OG, D-79106 Freiburg, Germany. E-mail: tonio.ball@uniklinik-freiburg.de

Oliver Speck and Tonio Ball contributed equally to this work.

Received for publication 18 June 2013; Revised 19 December 2013; Accepted 16 January 2014.

DOI 10.1002/hbm.22477

Published online 12 March 2014 in Wiley Online Library (wileyonlinelibrary.com).

Key words: amygdala; hippocampus; alveus; amygdala-hippocampal border; amygdalo–hippocampal interaction; high-resolution MRI; high-field MRI; structural MRI; anatomy; morphology

INTRODUCTION

Exact demarcation of the amygdala from the adjacent hippocampus is of great importance for studies addressing volumetric and functional questions regarding these brain structures. In the course of evolution, the morphology of the amygdala changed differentially between different primate species and humans, which possibly relates to the promotion of social behavior [Barger et al., 2007; Carlo et al., 2010; Rilling et al., 2011]. Variation in the volume and shape of the amygdala could therefore relate to the success of interpersonal interaction. The size and complexity of real-life and virtual social networks in adult humans have, for example, been shown to correlate with the volume of the amygdala [Bickart et al., 2011; Kanai et al., 2011]. Inter-individual volumetric differences of this structure have been shown to hold diagnostic value in a number of pathologies, such as in patients suffering from Alzheimer's disease, in whom the volume of the amygdala is decreased [Cuénod et al., 1993], or in autistic children, in whom it is, on the contrary, enlarged [Schumann et al., 2004]. Also, the shape of the amygdala may provide information on these and other pathological states [Kim et al., 2011]. Accurate delineation of the amygdalo-hippocampal border (AHB) is hence crucial for studies addressing the shape and volumetry of the amygdala, and new software tools have recently been developed to derive the spatial extent of the amygdala from magnetic resonance images (MRIs) [Collins and Pruessner, 2009; Morey et al., 2009]. An anatomical overview of the AHB region is given in Figure 1.

The amygdala has a fundamental role in emotional functions [LeDoux, 2007], including the processing of emotional memories [Adolphs et al., 1997]. Such processing has been shown to rely on strong interactions with the adjacent hippocampus [Bechara et al., 1995; Richardson et al., 2004; Vlachos et al., 2011], a crucial structure for explicit memory processing [Squire and Zola-Morgan, 1991]. For a better understanding of amygdalo-hippocampal interactions, many functional magnetic resonance imaging (fMRI) studies recently investigated spatially small-scaled differences of BOLD activation sites in the amygdalo-hippocampal region [Murty et al., 2011].

Delineating the boundaries between the amygdala and neighboring areas based on *in vivo* structural imaging of the human brain is difficult at present. Particularly the borderline between the amygdala and the hippocampal head has been a major issue in previous fMRI studies [Brierley et al., 2002; Malykhin et al., 2007; Pruessner et al., 2000; Watson et al., 1992; Konrad et al., 2009 for a review]. Diverse anatomic protocols exist to define the AHB, many of which rely on external landmarks (e.g., "arbitrary line linking the sulcus semilunaris with the inferior horn of the lateral ventricle," or "appearance of the corpora mamillaria on coronal slices") when direct anatomical landmarks of the AHB are not available [Konrad et al., 2009]. Delineating the amygdala from the hippocampus and other bordering areas using such indirect criteria, however, may lead to inaccuracies. Indeed, a meta-analysis [Ball et al., 2009a] using the probabilistic atlas system by Eickhoff et al. [2006] to reanalyze functional imaging studies, showed that 10% of all activation peaks assigned to the amygdala in the original studies actually lay with high probability in the hippocampus, and about 40% of all peaks were presumably located outside the entire amygdalohippocampal complex. This demonstrates the need for accurate and direct *in vivo* imaging techniques for anatomical delineation of the amygdala from surrounding brain structures in general, and from the hippocampus in particular.

The method of choice for high-resolution structural imaging in healthy subjects is magnetic resonance imaging (MRI). In recent years, imaging at ultra-high-field strength (7T and higher) has undergone rapid technical development, and it is becoming increasingly established for use in humans [Duyn, 2011]. 7T structural imaging has recently been employed for detailed visualization of several brain structures such as the hippocampus [Cho et al., 2010; Prudent et al., 2010; Thomas et al., 2008], the amygdala [Solano-Castiella et al., 2011], the visual cortex [Lee et al., 2011], and the midbrain dopaminergic system [Eapen et al., 2011]. Structural imaging at 7T has also proven beneficial over imaging at lower field strengths for studying anatomical changes in pathologies such as epilepsy [Madan and Grant, 2009], movement disorders [Abosch et al., 2010], and Alzheimer's disease [Kerchner et al., 2010]. The main advantage of employing stronger magnetic fields for structural imaging is that the level of tissue magnetization increases approximately linearly with magnetic field strength. This may permit better tissue delineation by increasing spatial resolution, decreasing scan time, or increasing the contrast-to-noise ratio. In addition, contrast-generating mechanisms such as susceptibility contrast or phase-contrast increase at higher fields with a supra-linear gain [Duyn, 2011]. Many high-field-related challenges for structural imaging, such as radio-frequency (RF)-field inhomogeneity and specific absorption rate (SAR) limitations, have successfully been addressed, in particular for brain imaging.

Here, we investigated the potential of 7T MRI to detect the structural border between the amygdala and the hippocampus by evaluating the visibility of both intra- (left vs. right) and inter-individual variations of the anatomical configuration of the AHB. We performed a comparison of *in vivo* 3T and 7T data acquired at the same spatial

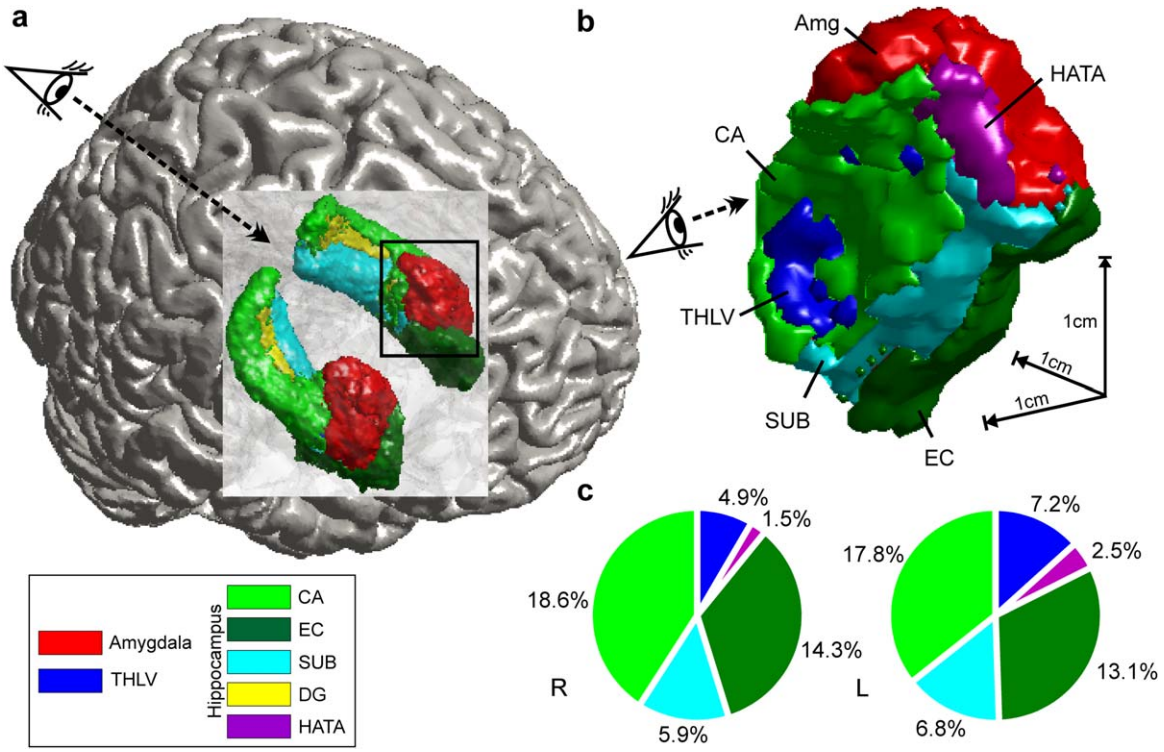

Figure 1.

Overview of the amygdalo-hippocampal border (AHB) based on the maximum probability maps by Eickhoff et al. (2006). (**a**) Anatomical orientation of the combined amygdalo–hippocampal complex in relation to a standard brain. 40.21% of the right and 40.13% of the left total amygdalar surface directly border upon the right and left hippocampi, respectively. Conversely, 13.93% and 13.81% of the respective right and left hippocampal surface border upon the right and left amygdala. About 12.45% of the right and 6.9% of the left amygdalar surface and 2.45% and 4.03% of the right and left hippocampus, respectively, directly adjoin the THLV. The left amygdala in (a), marked by a black square, is magnified and displayed from a different viewing angle in (**b**). Parts of the amygdala bordering upon the hippocampus and the THLV are color-coded according to the legend in (a). The spatial extension of the border areas are quantified in (**c**) as the percentage of the amygdala's total border area with the hippocampus and the THLV. See Supporting Information for further details. [Color figure can be viewed in the online issue, which is available at wileyonlinelibrary.com.]

resolution in the same subjects. To this end, we employed single-session MRI data sets, which require shorter image acquisition times than in previous 3T studies averaging across multiple scans [Bonnici et al., 2012; Entis et al., 2012; Konrad et al., 2009; Saygin et al., 2011]. Reduction of imaging time is an important goal which may alleviate patient time and effort in a clinical context [Entis et al., 2012; Hennig et al., 1986; Tsao, 2010] and increase the number of healthy subjects who can be imaged in a limited amount of experimental time.

MATERIALS AND METHODS

Subjects

Six male subjects between 24 and 28 years of age participated in this study. None of them had a history of neurological or psychiatric dysfunctions. All subjects were right-handed and provided written informed consent.

MRI Acquisition and Visualization

T1

For the 7T *in vivo* images shown in Figures 2–7, whole-head 3D volumes were acquired on a whole-body Siemens 7T system with T1-weighted MPRAGE (TR, 2,600 ms; TE, 3.27 ms; TI, 1,050 ms; flip angle, 5°; FOV, 224 × 224 mm^2; bandwidth, 130 Hz/Px; 320 slices; whole-brain acquisition time, 17:08 min) and proton-density-weighted GE sequences (TR, 2,290 ms; TE, 3.27 ms; flip angle, 5°; FOV, 224 × 224 mm^2; bandwidth, 130 Hz/Px) with an isotropic voxel resolution of 0.5 mm^3. To account for the bias-field due to RF-inhomogeneity and for residual T2* effects, the MPRAGE images were divided by the GE images and thresholded [Lüsebrink et al., 2012; Van de Moortele et al., 2009]. Because of blood flow effects inside arteries, the corresponding voxel values lie below threshold and thus appear as black voids inside the vessels. This procedure was applied for whole-brain visualization. Nevertheless, for the analyses

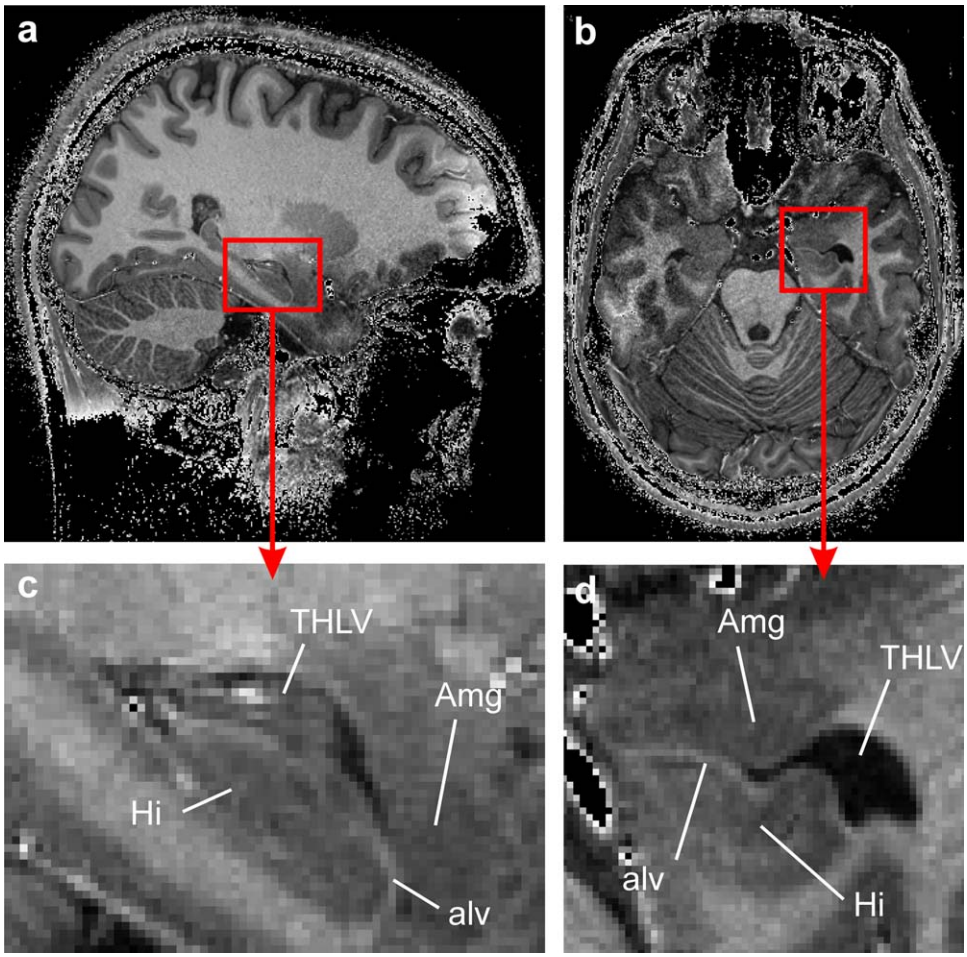

Figure 2.

The amygdala (Amg) and the hippocampus (Hi) in the medio-temporal lobe of S1. (**a**) T1-weighted *in vivo* MRI in the sagittal plane. The amygdalo-hippocampal area, marked by a red square, is magnified in (**c**). The corresponding axial view is displayed in (**b**) and the magnified AHB area is shown in (**d**). The border between the amygdala and the hippocampus formed by the temporal horn of the lateral ventricle (THLV) and the alveus (alv) can be clearly seen. [Color figure can be viewed in the online issue, which is available at wileyonlinelibrary.com.]

focusing on the amygdala and the AHB region, additional GE images would not have been required.

For S1 and S2, we further acquired T1-weighted MRI volumes at 3T with (i) an isotropic resolution of 1 mm^3; (TR, 2,500 ms; TE, 4.77 ms; TI, 1,100 ms; flip angle, 7°; FOV, 256 × 256 mm^2; bandwidth, 140 Hz/Px; 192 slices; whole-brain acquisition time, 9:20 min) and (ii) 0.5-mm^3; isotropic resolution (TR, 2,540 ms; TE, 2.97 ms; TI, 1,050 ms; flip angle, 7°; FOV, 224 × 224 mm^2; bandwidth, 172 Hz/Px; 288 slices; whole-brain acquisition time, 14:16 min).

T2 and T2*

The T2*-weighted image in Figure 8 was obtained from S1 at 7T with a 32-channel head coil and a voxel resolution of 0.33 × 0.33 × 1 mm^3; in 2D multi-slice gradient echo acquisition (TR, 875 ms; TE, 18 ms; flip angle, 45°; FOV, 212 × 212 mm^2; bandwidth, 60 Hz/Px; 30 slices; acquisition time 7:53 min).

We further acquired T2-weighted MRI volumes with an isotropic resolution of 0.4 × 0.4 × 1 mm^3; (TR, 8,000 ms; TE, 86 ms; flip angle, 90°; FOV, 198 × 212 mm^2; bandwidth, 178 Hz/Px; 44 slices; acquisition time, 5:45 min) and 0.4 × 0.4 × 2 mm^3; (TR, 8,000 ms; TE, 83 ms; flip angle, 90°; FOV, 198 × 212 mm^2; bandwidth, 178 Hz/Px; 44 slices; acquisition time, 5:45 min) for S1 and S2. However, as these images did not reveal more detail on the AHB than T1-weighted MRIs in the present study, we further focused on the T1 images, which can readily be acquired with a high isotropic resolution.

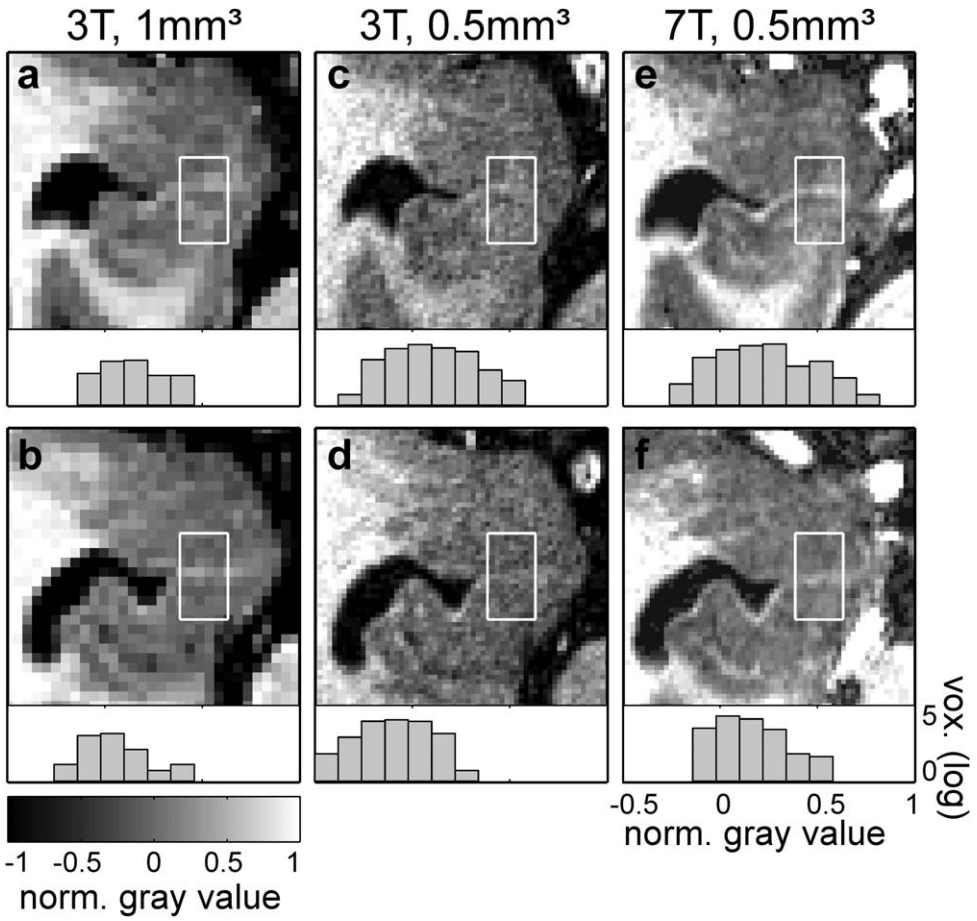

Figure 3.

Comparison of T1-weighted, normalized MRIs of the AHB acquired at 3T with a 1-mm^3 isotropic resolution (**a,b**), at 3T with a 0.5-mm^3 (**c,d**) and at 7T with a 0.5-mm^3 resolution (**e,f**). The histograms below the MRIs show the distribution of the voxel intensities in the part of the AHB highlighted by the white boxes. Although the shape of the alveus may be discernible in 3T 1-mm (b) and 0.5-mm (d) images, as is shown here for S1, it is considerably more distinct in the 7T 0.5-mm images (f). While the AHB in (c) at 0.5-mm 3T can be scarcely distinguished, if at all, it is clearly visible in the corresponding 7T MRI (e).

MRI Visualization

Based on previous findings from volumetric studies on the borders of the amygdala [Brierley et al., 2002; Konrad et al., 2009; Pruessner et al., 2000; Schumann et al., 2004; Watson et al., 1992] and the brain atlas by Mai et al. [2007], MRIs were visually inspected for corresponding anatomical septa in axial, sagittal, and coronal sectional planes visualized using Matlab-based (R2009a, Mathworks) software developed in our lab.

The contrast of the MRIs was optimized for improved figure quality using the 'imadjust' algorithm in Matlab (R2009a, Mathworks). This step was however only used for visualization, and it was not necessary/used for clear and reliable recognition of the AHB or for the contrast-to-noise analysis. To provide an anatomical point of reference for the visualization of the AHB, the temporal horns of the lateral ventricles (THLV) were semiautomatically segmented using a gray-value-threshold-based growth algorithm (26 direction 3D flood-fill) and rendered in blue.

3T-7T Comparison

To determine the effects of magnetic field strength on the imaging quality of the AHB, we compared T1-weighted MRIs of the AHB with a 0.5-mm^3 isotropic resolution acquired at 7T and 3T in S1 and S2 (acquisition parameters are described in the previous paragraph).

For comparisons of the alveus contrast relative to the adjacent gray matter in 3T and 7T data, we calculated the contrast for the alvear part of the AHB (C_{alv}) as

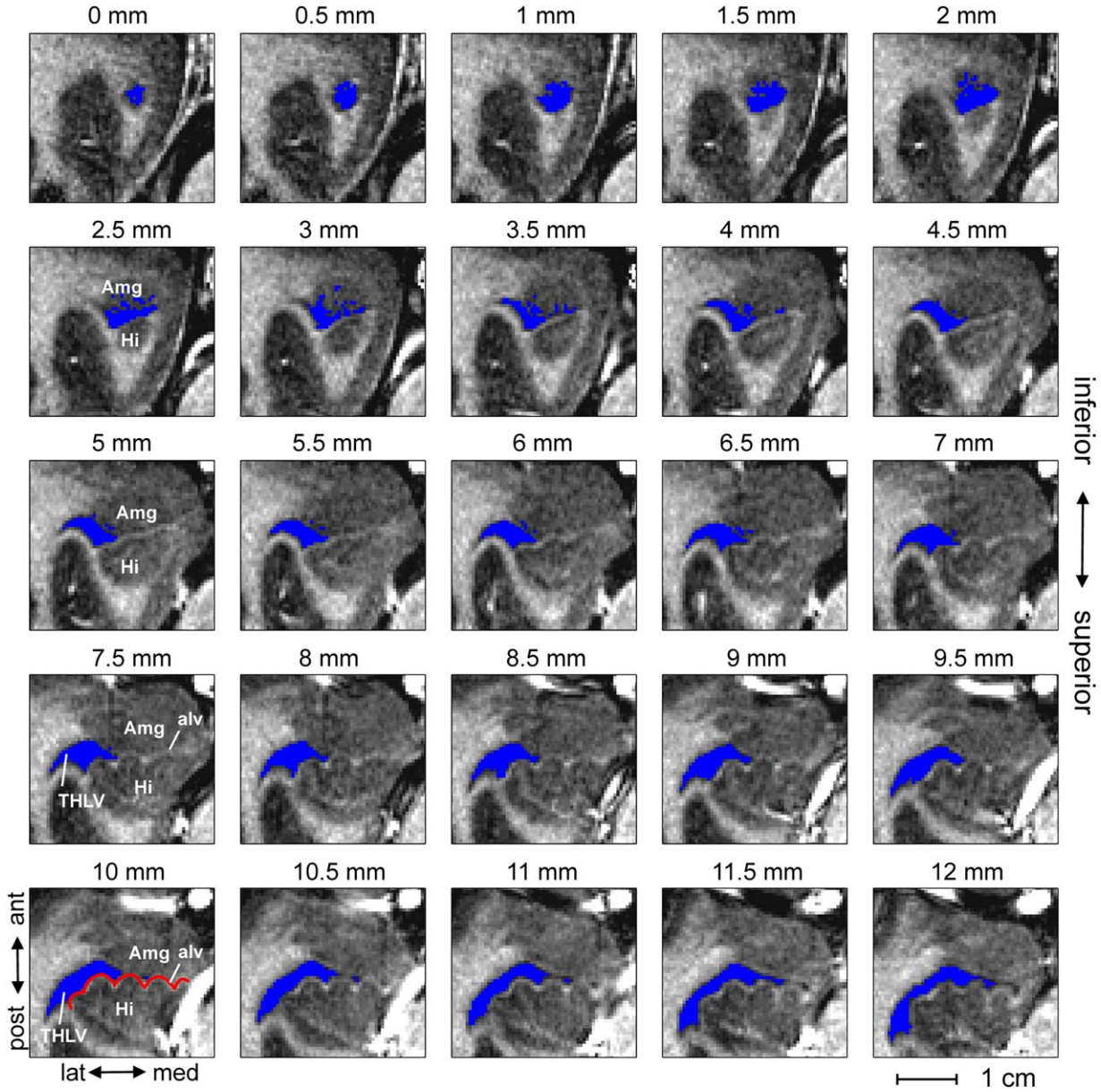

Figure 4.

A 7T axial image sequence of the AHB region in steps of 0.5 mm and with a 0.5-mm^3 isotropic resolution (S1). The amygdala (Amg) is separated from the hippocampus (Hi) by the temporal horn of the lateral ventricle (THLV, blue) and by the white matter tracts forming the alveus (alv). Above each panel, the distance to the inferior-most section is indicated. The AHB can be well seen throughout all sections. In the axial plane, the anterior border of the amygdala, formed by the white matter, can be clearly delineated in the inferior part of the amygdala up to 5 mm superior to the inferior amygdalar pole. As expected, the medial-most parts of the AHB, where the amygdala directly borders the hippocampus and the entorhinal cortex, were most difficult to discern. In several slices, the typical arcade-shaped course of the AHB can be seen (an example is marked by a red line in the 10-mm panel). [Color figure can be viewed in the online issue, which is available at wileyonlinelibrary.com.]

$$C_{alv} = \frac{(i_{alv} - i_{wm})}{(i_{gm} - i_{wm})}, \quad (1)$$

where i_{alv} is the mean intensity of the alveus, i_{gm} the mean intensity of gray matter, and i_{wm} the mean intensity of white matter. In this way, values of i_{alv}, i_{gm}, and i_{wm} were computed in 12 consecutive axial slices. Mean gray-matter intensities were obtained by averaging voxel intensities from 21 voxels (5.25 mm^2) of the amygdala gray matter close to the alveus. Likewise, mean white matter

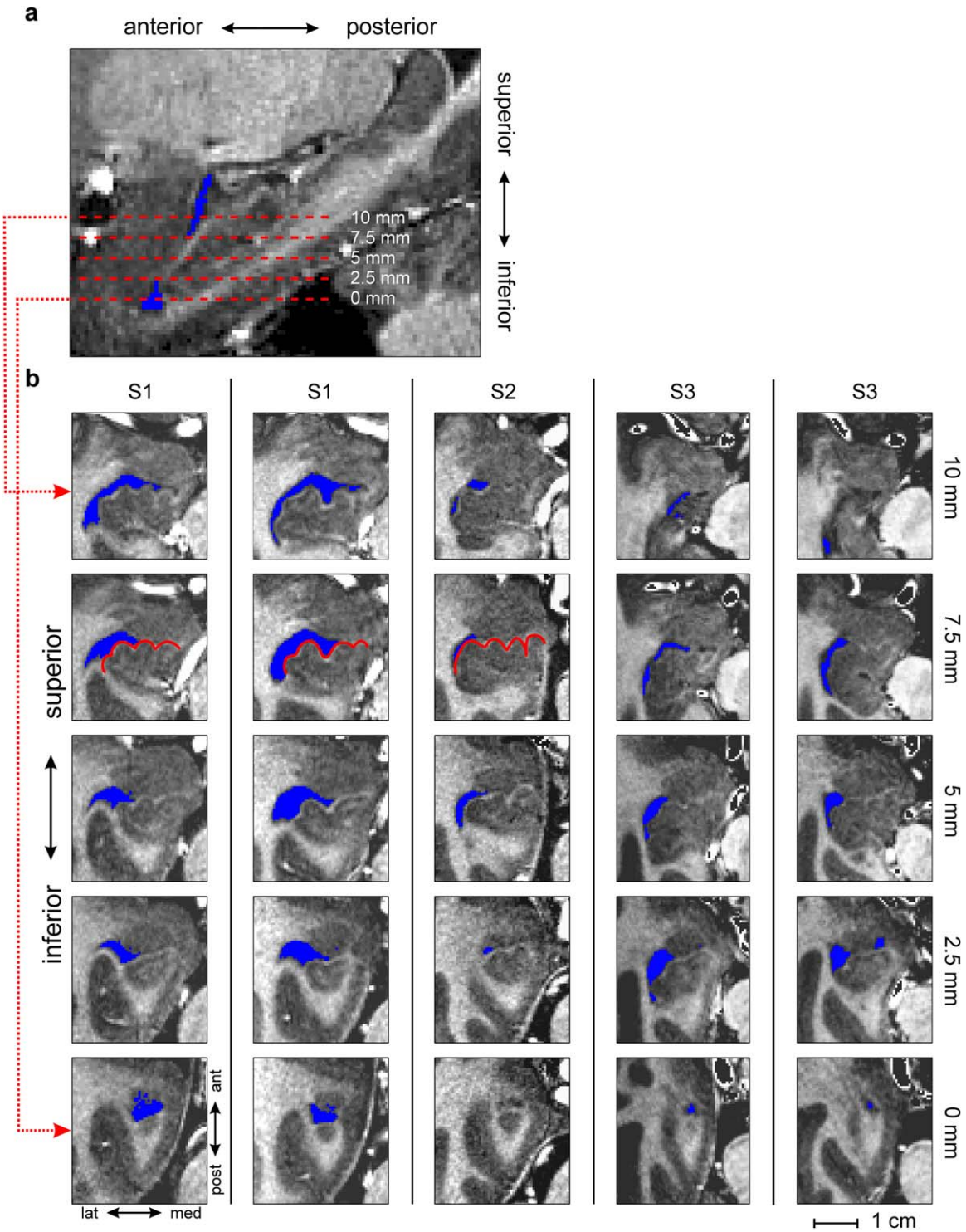

Figure 5.

Variability in the shape of the alveus and the THLV. (**a**) Sagittal section through the AHB area of S1. (**b**) Axial images corresponding to the positions are marked by red dashed lines in (a). Images from the left hemisphere (S1, first column and S3, fourth column) are mirrored for better comparison. The variability of the alveus becomes especially obvious in the first three panels of the second row in (b), where the alveus is marked in red. [Color figure can be viewed in the online issue, which is available at wileyonlinelibrary.com.]

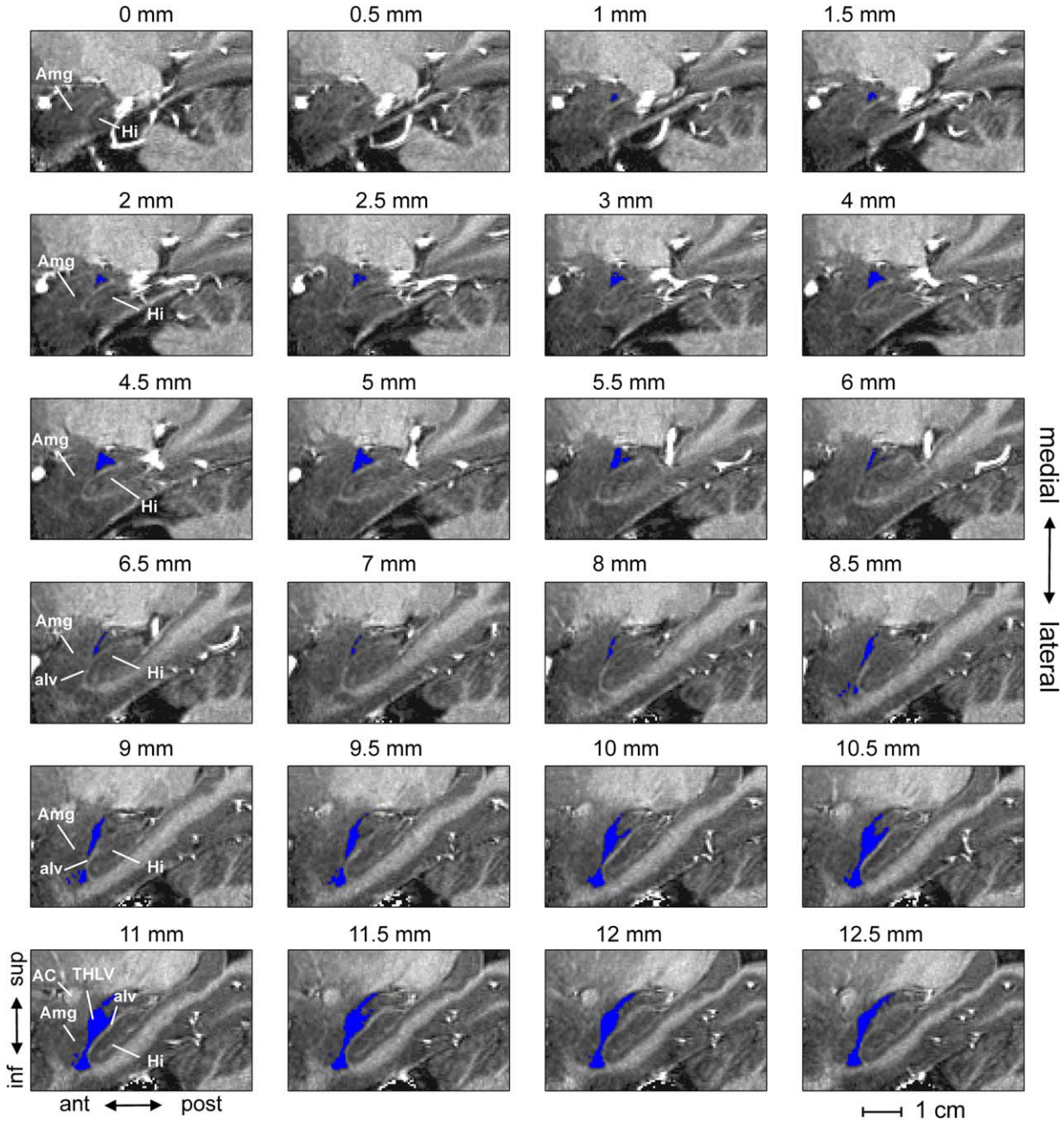

Figure 6.

A 7T sagittal image sequence of the AHB region in steps of 0.5 mm and with a 0.5-mm^3 isotropic resolution (S1). The amygdala and the hippocampus are separated by the THLV (in blue) and by the adjacent white matter of the alveus. [Color figure can be viewed in the online issue, which is available at wileyonlinelibrary.com.]

intensities were calculated from 21 voxel of white matter from the medial temporal lobe close to the amygdala. The alvear white matter strand was manually segmented both in 3T and 7T data, and the mean, normalized voxel intensity of the segmented alveus in each slice was calculated, providing a measure of how close the voxel intensity of the alveus was to white matter.

According to Eq. (1), the normalized data yields contrast values of 1 for "pure" white-matter structures and values of 0 for "pure" gray matter. Because the alveus is an axon fiber bundle, voxel intensities in this structure should be close to those of white matter. To address C_{alv} differences in 7T 0.5-mm^3 and 3T 0.5-mm^3 isotropic images, we determined the mean and the standard deviation from the C_{alv}

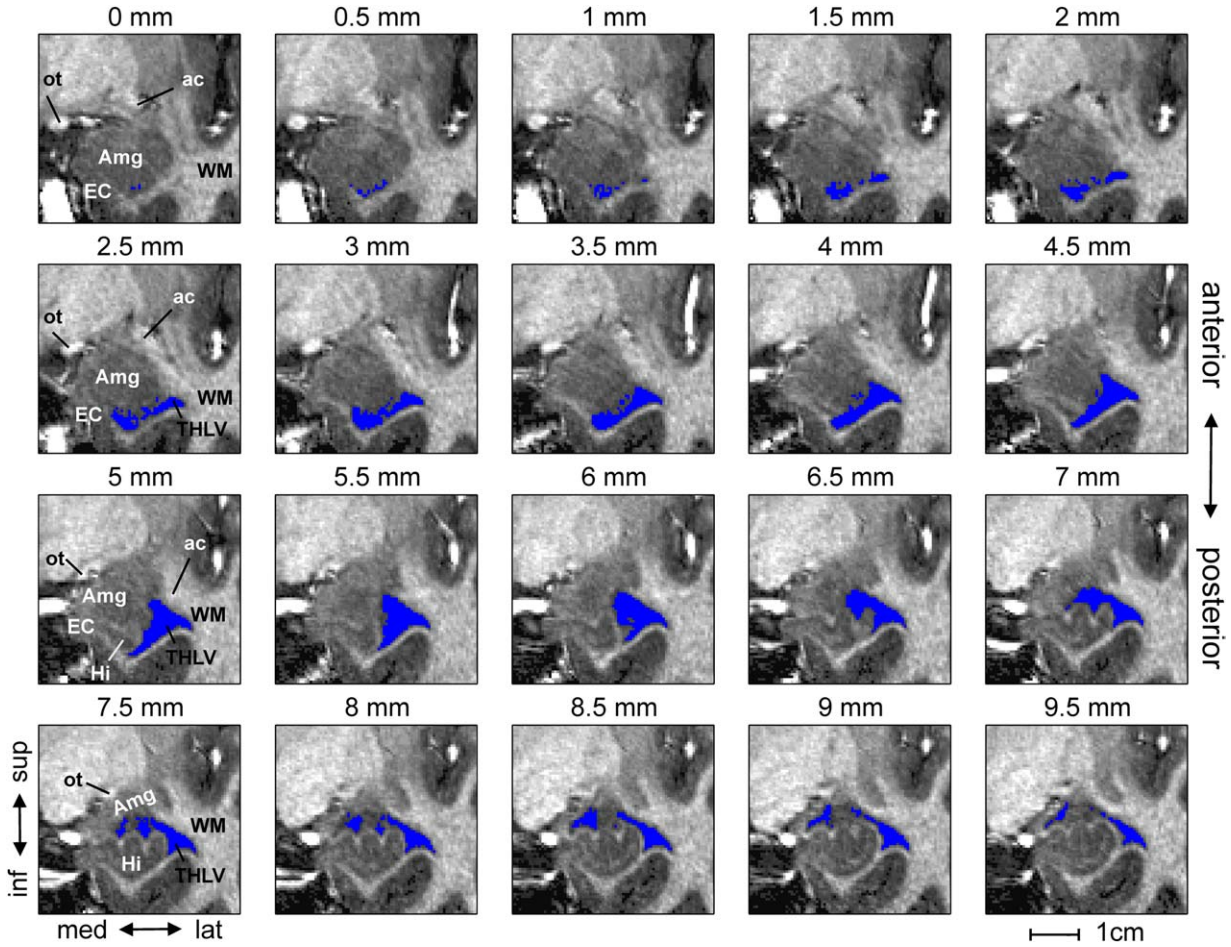

Figure 7.

A 7T coronal image sequence of the AHB region in steps of 0.5 mm and with a 0.5-mm^3 isotropic resolution (S1), showing also the optical tract (ot), the anterior commissure (ac), the subamygdaloid white matter (WM), and the entorhinal cortex (EC). The arcade-shaped course of the AHB can be seen in the more posterior slices (bottom row of the panels). [Color figure can be viewed in the online issue, which is available at wileyonlinelibrary.com.]

values of the respective 12 sections in the 7T and 3T images.

The signal contrast of the alveus C_{alv} quantifies the alvear voxel intensities without taking into account the image noise level. C_{alv} measures alone are hence not informative about how robustly the alveus can be discerned from the adjacent gray matter, and a measure of the contrast-to-noise relation is required. Generally, the contrast-to-noise ratio (CNR) quantifies the ratio of contrast, i.e., intensity differences between structures of interest and general image noise. In a subsequent analysis, we assessed the CNR by relating the contrast between alvear and gray-matter signal amplitudes and background noise according to

$$CNR_{alv} = \frac{(E[i_{alv}] - E[i_{gm}])^2}{2(Var[i_{alv}] + Var[i_{gm}])}, \quad (2)$$

where E denotes the mean value and Var the variance.

RESULTS

Brain Structures of the AHB

In the present study, the anatomical extent of the AHB was for the first time systematically documented in coronal, axial, and sagittal planes.

The AHB is formed by the characteristic cerebrospinal fluid (CSF) of the THLV and by the alveus, a sheet of white matter which shows high signal intensity compared to that of gray matter in the T1-weighted data. As is illustrated in Figure 2, both structures can be clearly visualized and distinguished in 7T MRI. In particular, the T1-weighted images of the AHB area have revealed the alvear border between the amygdala and the hippocampus, distinctly visible as a fine layer of white matter in medial parts of the AHB (Figs. 2–7). From there, the THLV extends laterally and appears

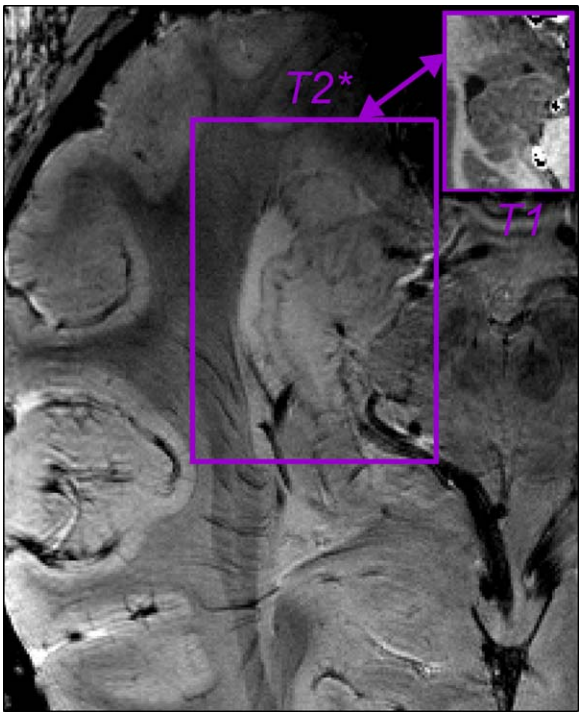

Figure 8.
High-resolution T2* image of the AHB in a section parallel to the hippocampal body of S1 shown in an axial view. The inset comprises approximately the same section of the same subject in T1-weighted data. In-plane resolution of the T2* image is 0.2 × 0.2 mm^2 with a slice thickness of 2 mm. [Color figure can be viewed in the online issue, which is available at wileyonlinelibrary.com.]

characteristically dark. Throughout all sections, the alveus remains consistently visible as a sheet of white matter, extending from the uncal gyrus towards the ventral surface of the THLV. The increased topographic detail of 7T imaging with a 0.5-mm resolution suits well for imaging the alveus, which is only 1–3 voxels (0.5–1.5 mm) thick.

Comparison of 3T and 7T Data

It can be seen from visual inspection that, as expected, 1-mm^3 isotropic imaging at 3T provided less detail of the alveus than MRI with a 0.5-mm resolution (Fig. 3). With high-resolution imaging at 0.5 mm, the shape and extent of the alveus could be better traced in images acquired at 7T than 3T (compare second and third column in Fig. 3). This is also reflected in the consistently higher alveus contrasts C_{alv} of the 0.5-mm 7T than in 0.5-mm 3T MRIs in both S1 and S2: on average, C_{alv} of the 12 analyzed sections of the AHB were 0.35 ± 0.08/0.19 ± 0.09 for the 7T/3T data in S1, and 0.40 ± 0.06/0.18 ± 0.07 for the 7T/3T data in S2. The alveus CNR_{alv} were also higher in 7T than in 3T images in both subjects: mean CNR_{alv} for the 12 sections were 10.0 ± 6.0/1.24 ± 0.85 in 7T/3T images in S1, and 2.58 ± 1.32/0.48 ± 0.38 in 7T/3T images in S2.

Variability of the AHB

The appearance of the THLV varied from a small, prolonged cavity to a larger moon-shaped structure, depending on the axial position of the MRI section and the individual anatomy, as could be observed both in *in vivo* and post mortem brains (Fig. 5 and Supporting Information Fig. 1). Similarly, the course of the alveus varied substantially, following the intrusions of the undulating hippocampus and the outlines of the THLV. Differences could be observed between the AHB in the right and left hemisphere of individuals as well as between subjects.

Selection of Sectional Planes

Axial images were particularly well suited to determine the AHB, as large parts of both the amygdala and the hippocampus were visible throughout all layers (Fig. 4). Especially in the superior axial slices through the amygdala, the arcade-shaped course of the AHB was clearly visible in all subjects (examples marked by red lines in Figs. 4 and 5). In the axial images, it also became evident that the shape and extent of the alveus and the THLV at the level of detail revealed by 7T imaging is highly variable both intra- (i.e., right vs. left hemisphere) and inter-individually (Fig. 5 and Supporting Information Fig. 1). No uniform standard map can therefore be expected to accurately fit to the individual anatomy.

The sagittal sections were most informative for the lateral part of the AHB, roughly to the level where the THLV ended; see Figure 6 for a sequence of sagittal MRIs. The coronal sections proved beneficial for delineating the lateral and medial extensions of the amygdala including the borders to the optical tract and the anterior commissure, among many other structures (Fig. 7). The arcade-shaped course of the AHB was, again, very clear in posterior coronal images (Fig. 7, lower panels).

Other Amygdalar Borders and Subnuclei

Some other external borders of the amygdala, e.g., to parts of the adjacent cortex, were clearly visible in the single-scan MRIs. Other neighboring structures, such as the basal ganglia, were difficult or impossible to visually distinguish from the amygdala. Also the individual subnuclei of the amygdala, which is a topic of increasing interest in recent human imaging [Bach et al., 2011; Ball et al., 2007; Goossens et al., 2009], could not be clearly delineated from each other. MRI optimized for these structures will likely require averaging data from multiple sessions (see Discussion). However, since the aim of the present study was to delineate the AHB based on single-session MRI

data, in the following we will exclusively focus on this particular border of the amygdala.

T2*-Weighted MRI

T2*-weighted MRIs of the AHB area are shown in Figure 8 as an example of images with alternative tissue contrasts. These 2D images have a substantially higher in-plane resolution than the T1-weighted 3D data (200 μm vs. 500 μm; more than six times smaller in-plane voxel size), albeit with a 4 times higher slice thickness. Like in the T1-weighted images, the AHB can be seen very clearly in the axial slices, where it is approximately perpendicular to slice orientation.

DISCUSSION

This study addresses the question whether the AHB can be reliably visualized in single-session T1 data sets at 7T, as compared with previous 3T studies relying on averaging across data sets from multiple sessions [Bonnici et al., 2012; Entis et al., 2012; Konrad et al., 2009; Saygin et al., 2011].

Anatomically, about 40% of the total surface of the amygdala adjoins to the anterosuperior hippocampus in the AHB region (Fig. 1). Medially, the AHB is formed by the alveus, which divides the amygdala from the hippocampus. More laterally on the AHB appears the THLV, covered by the alveus on the hippocampal side (see Fig. 2). The alveus is a sheet-like band of white matter that contains afferent and efferent projections to and from the hippocampal formation. Alvear neurons of the hippocampus and the subiculum form the main efferent path of these structures, entering the fimbria hippocampi (fornicis), which arises at the uncus and merges into the crus fornicis. An important source of afferent fibers is the septum [Duvernoy, 1987].

The alveus is a fine structure, and superior image quality and high spatial resolution are needed to discern it from the surrounding gray matter. When comparing the potential of structural MRI at different field strengths to visualize the AHB, we found that ultra-high-field neuroimaging at 7T has marked advantages over 3T for discerning the fine anatomical details of the AHB (Fig. 3). Improved separation of the alvear white matter at 7T is reflected in the image contrast and the CNR of the AHB area, which were both higher in the 7T than in the 3T MRI data. This is consistent with theoretical expectations and experimental evidence that superior image contrast can be achieved in high-field MRI [Duyn, 2011]. The amount of topographical detail in 7T images in the present study is in accordance with the recent findings on hippocampal anatomy by Cho et al. [2010]. Precise and unambiguous demarcation of the AHB is a prerequisite for accurate volumetric and shape analyses, as well as for functional imaging in the AHB area [Brierley et al., 2002; Konrad et al., 2009; Malykhin et al., 2007].

Although quantitative volumetry of the amygdala and the hippocampus was not the goal of the current work, it suggests that volumetric differences can be expected in volumes derived from segmentations of MRIs acquired at 7T with those acquired at lower field strengths. Future work is required to quantify how the level of anatomical clarity influences the outcome of automated and manual segmentations, and whether and to what extent volumetric measures are affected.

In the individual brain, distinctive delineation of the AHB may help to improve volumetric studies and to resolve current controversies, for example, regarding pathological volume alterations of the amygdala and the hippocampus in depressive patients, as discussed in Campbell et al. [2004] and Bellani et al. [2011]. Individual *in vivo* imaging may also prevent wrong anatomical assignments of hippocampal responses to the amygdala, and *vice versa* [Ball et al., 2009a]. In functional imaging of individual brains, anatomical high-resolution T1-weighted images constitute the basis for assigning BOLD activation sites in lower-resolution functional T2* images to corresponding anatomical structures. Clear delineation of the individual AHB in the anatomical images acquired at 7T, as was done in the present study, can therefore be expected to increase the assignment accuracy of BOLD responses in individuals. Furthermore, improved coregistration procedures may be needed to gain more accuracy in aligning the functional image with the corresponding anatomical image [Ball et al., 2009b].

An important finding of the present study is that the shape and extent of the AHB vary substantially between subjects and hemispheres (Fig. 5 and Supporting Information Fig. 1). These variations were present both in MRIs from *in vivo* (Fig. 5) and post mortem (Supporting Information Fig. 1) brains, the latter partly obtained from the open-source datasets provided by Yushkevich et al. [2009]. Our results illustrate the great potential of post mortem imaging for high-resolution anatomical studies (for an in-depth discussion on imaging human post mortem brains, see Yang et al., 2013). Macroscopic properties of the anatomical interface between the amygdala and the hippocampus may have functional relevance for neural communication between the two structures. For instance, strong folding of the hippocampal gyri in the AHB area and hence enlarged contact area of the gyral surface to the amygdala may provide a broader anatomical communication channel between the amygdala and the hippocampus, and possibly facilitate the interaction between the two. Conversely, a larger THLV may constrain the available area for reciprocal amygdalo-hippocampal fiber projections. Future studies are needed to clarify whether the individual variability of the AHB as shown here correlates with functional differences related to amygdalo-hippocampal communication. To this purpose, the adaptation of algorithms to the AHB that quantify the

gyrification strength and that have been previously developed for the neocortex [e.g., Luders et al., 2006] would allow for correlating gyrification measures with cognitive and behavior parameters in healthy and pathological conditions.

The large variability of the AHB also imposes limitations on the accuracy in delineating the amygdala from the hippocampus that can be achieved by standard atlas systems, which do not take individual anatomy into account. As the structure of any standard AHB cannot closely match all individual variations in this region, individual imaging is required whenever maximal anatomical accuracy is desired. In addition, this variability, if not compensated for by advanced normalization techniques, limits the accuracy in any structural or functional group analysis.

In addition to the hippocampus, the amygdala has close spatial relations with several other neighboring gray-matter structures. According to the brain atlas by Mai et al. [2007], these include cortical areas, such as the ambiens gyrus, the cortex of the enthorhinal area, parts of the uncus hippocampi, the parahippocampal gyrus, the temporal part of the piriform cortex, the perirhinal cortex, parts of the semilunar gyrus, parts of the ventral insular cortex and of the claustrum, and transitions towards basal ganglia structures. The latter are especially hard to delineate, since the centro-medial amygdala has a microstructure similar to that of the adjacent basal ganglia [Swanson and Petrovich, 1998], i.e., the internal and external globus pallidus and the putamen (all superior to the amygdala). Evaluation of the potential of different MRI techniques to distinguish the amygdala from these areas is under way and clearly an important topic for further research. In this context, averaging multiple 7T scans, similar to previous 3T studies [Bonnici et al., 2012; Entis et al., 2012; Konrad et al., 2009; Saygin et al., 2011], is a promising approach, as is exploitation of different structural image contrasts [Hu et al., 2011] and optimized image reslicing [Brierley et al., 2002]. Investigations on the role of field strength for visualizing amygdalar borders in general and of the AHB in particular is a further topic of practical importance [Konrads et al. 2009].

The T1 images acquired in this study are not quantitative T1 maps. However, they were mainly T1-weighted, as other potential sources of image contrast were accounted for by the correction (division) with the 3D GE data. The T1-weighted (MPRAGE) and short TE 3D GE data share identical sensitivity to B1 field inhomogeneity (same flip angle), T2* (same TE), and proton density. Therefore, the division of both data sets results in almost exclusively T1-weighted images although no T1 quantification is available. Future studies may use methods such as MP2RAGE to extend this acquisition to quantitative T1 maps. Apart from T1, T2*-weighted images also unveiled much anatomical information about the AHB region. The amount of structural detail in T2* (Fig. 8) is comparable to what can be observed in T1, as is discussed in earlier sections. The good visibility of the AHB in T2* images may be due to their strong sensitivity to iron [Anderson et al., 2001], which is particularly abundant in the white matter of the AHB region [Connor et al., 1990]. A crucial advantage of T2* high-resolution functional imaging is that it would allow solving the aforementioned problem of coregistration. A disadvantage, however, is the relatively long time required to obtain such images, e.g., the acquisition of the T2* MRIs in Figure 8 with a fast low-angle shot (FLASH) technique took several minutes for a whole-brain data set. Nevertheless, acquisition times can be reduced such as by imaging smaller ROIs or using segmented echo-planar imaging (EPI) techniques [Jesmanowicz et al., 1998; Menon and Goodyear, 1999]. High-resolution single-shot EPI-based fMRI at 7T has recently been demonstrated [Heidemann et al., 2012; Hoffmann et al., 2009; Polimeni et al., 2010]. Alongside T2*, quantitative susceptibility mapping (QSM) is even more sensitive to detect local variations in iron content, being thus a promising technique to facilitate further improvements to visualization of the AHB.

CONCLUSIONS

In summary, we were able to visualize the structural border between the amygdala and the hippocampus and its variability with great spatial detail using high-resolution structural imaging at 7T. The present approach offers a solution to the problem of anatomical ambiguity in the AHB region as it can be encountered at a lower resolution. A practical limitation to widespread usage of 7T MRI to delineate the details of the AHB region at present, however, is that 7T scanners are not as widely available as 3T and 1.5T MRI systems. Elucidating the subtleties of the AHB region can still be of great value as researchers increasingly move toward higher field strengths and advance the limits of multi-modal imaging approaches which may benefit greatly from the improved anatomical information derivable from 7T data, as described here for the AHB region. Imaging at high field strengths thus is a promising tool to derive detailed anatomical information about the human brain, and it may be of value for neuroradiologic assessment of disorders such as temporal lobe epilepsy and for structural and functional studies in neurological patients as well as in healthy subjects.

ACKNOWLEDGMENTS

The authors thank Olga Iljina for her comments on the manuscript.

REFERENCES

Abosch A, Yacoub E, Ugurbil K, Harel N (2010): An assessment of current brain targets for deep brain stimulation surgery with susceptibility-weighted imaging at 7 tesla. Neurosurgery 67:1745–1756.

Adolphs R, Cahill L, Schul R, Babinsky R (1997): Impaired declarative memory for emotional material following bilateral amygdala damage in humans. Learn Mem 4:291–300.

Amunts K, Kedo O, Kindler M, Pieperhoff P, Mohlberg H, Shah NJ, Habel U, Schneider F, Zilles K (2005): Cytoarchitectonic mapping of the human amygdala, hippocampal region and entorhinal cortex: Intersubject variability and probability maps. Anat Embryol 210:343–352.

Anderson LJ, Holden S, Davis B, Prescott E, Charrier CC, Bunce NH, Firmin DN, Wonke B, Porter J, Walker JM, Pennel DJ (2001): Cardiovascular T2-star (T2*) magnetic resonance for the early diagnosis of myocardial iron overload. Eur Heart J 22:2171–2179.

Bach DR, Behrens TE, Garrido L, Weiskopf N, Dolan RJ (2011): Deep and superficial amygdala nuclei projections revealed in vivo by probabilistic tractography. J Neurosci 31:618–623.

Ball T, Rahm B, Eickhoff SB, Schulze-Bonhage A, Speck O, Mutschler I (2007): Response properties of human amygdala subregions: Evidence based on functional MRI combined with probabilistic anatomical maps. PloS One 2:e307.

Ball T, Derix J, Wentlandt J, Wieckhorst B, Speck O, Schulze-Bonhage A, Mutschler I (2009a): Anatomical specificity of functional amygdala imaging of responses to stimuli with positive and negative emotional valence. J Neurosci Methods 180:57–70.

Ball T, Mutschler I, Jäger D, Otte M, Schulze-Bonhage A, Hennig J, Speck O, Schreiber A (2009b): Elastic registration of functional MRI data to sensorimotor cortex. In: Sloten J, Verdonck P, Nyssen M, Haueisen J, editor. 4th European Conference of the International Federation for Medical and Biological Engineering. Berlin, Heidelberg: Springer Berlin Heidelberg. pp 684–688.

Barger N, Stefanacci L, Semendeferi K (2007): A comparative volumetric analysis of the amygdaloid complex and basolateral division in the human and ape brain. Am J Phys Anthropol 134:392–403.

Bechara A, Tranel D, Damasio H, Adolphs R, Rockland C, Damasio AR (1995): Double dissociation of conditioning and declarative knowledge relative to the amygdala and hippocampus in humans. Science 269:1115–1118.

Bellani M, Baiano M, Brambilla P (2011): Brain anatomy of major depression II. Focus on amygdala. Epidemiol Psychiatr Sci 20: 33–36.

Bickart KC, Wright CI, Dautoff RJ, Dickerson BC, Barrett LF (2011): Amygdala volume and social network size in humans. Nat Neurosci 14:163–164.

Bonnici HM, Chadwick MJ, Kumaran D, Hassabis D, Weiskopf N, Maguire EA (2012): Multi-voxel pattern analysis in human hippocampal subfields. Front Hum Neurosci 6:290.

Brierley B, Shaw P, David AS (2002): The human amygdala: A systematic review and meta-analysis of volumetric magnetic resonance imaging. Brain Res Rev 39:84–105.

Campbell S, Marriott M, Nahmias C, MacQueen GM (2004): Lower hippocampal volume in patients suffering from depression: A meta-analysis. Am J Psychiatry 161:598–607.

Carlo CN, Stefanacci L, Semendeferi K, Stevens CF (2010): Comparative analyses of the neuron numbers and volumes of the amygdaloid complex in old and new world primates. J Comp Neurol 518:1176–1198.

Cho Z-H, Han J-Y, Hwang S-I, Kim D, Kim K-N, Kim N-B, Chi JG, Park CW, Kim YB (2010): Quantitative analysis of the hippocampus using images obtained from 7.0 T MRI. Neuroimage 49:2134–2140.

Collins DL, Pruessner JC (2009): Towards accurate, automatic segmentation of the hippocampus and amygdala from MRI. Med Image Comput Comput Assist Interv 12:592–600.

Connor JR, Menzies SL, Martin SMS, Mufson EJ (1990): Cellular distribution of transferrin, ferritin, and iron in normal and aged human brains. J Neurosc Res 27:595–611.

Cuénod CA, Denys A, Michot JL, Jehenson P, Forette F, Kaplan D, Syrota A, Boller F (1993): Amygdala atrophy in Alzheimer's disease. An in vivo magnetic resonance imaging study. Arch Neurol 50:941–945.

Duvernoy HM (1987): The Human Hippocampus: Functional Anatomy, Vascularization and Serial Sections with MRI. Berlin, Heidelberg: Springer Berlin Heidelberg.

Duyn JH (2011): The future of ultra-high field MRI and fMRI for study of the human brain. Neuroimage 62:1241–1248.

Eapen M, Zald DH, Gatenby JC, Ding Z, Gore JC (2011): Using high-resolution MR imaging at 7T to evaluate the anatomy of the midbrain dopaminergic system. Am J Neuroradiol 32:688–694.

Eickhoff SB, Heim S, Zilles K, Amunts K (2006): Testing anatomically specified hypotheses in functional imaging using cytoarchitectonic maps. Neuroimage 32:570–582.

Entis JJ, Doerga P, Barett LF, Dickerson BC (2012): A reliable protocol for the manual segmentation of the human amygdala and its subregions using ultra-high resolution MRI. Neuroimage 60:1226–1235.

Goossens L, Kukolja J, Onur OA, Fink GR, Maier W, Griez E, Schruers K, Hurlemann R (2009): Selective processing of social stimuli in the superficial amygdala. Hum Brain Mapp 30:3332–3338.

Heidemann RM, Ivanov D, Trampel R, Fasano F, Meyer H, Pfeuffer J, Turner R (2012): Isotropic submillimeter fMRI in the human brain at 7 T: Combining reduced field-of-view imaging and partially parallel acquisitions. Magn Reson Med 68:1506–1516.

Hennig J, Nauerth A, nd Friedburg H (1986): RARE imaging: A fast imaging method for clinical MR. Magn Reson Med 3:823–833.

Hoffmann MB, Stadler J, Kanowski M, Speck O (2009): Retinotopic mapping of the human visual cortex at a magnetic field strength of 7T. Clin Neurophysiol 120:108–116.

Hu S, Coupé P, Pruessner JC, Collins DL (2011): Appearance-based modeling for segmentation of hippocampus and amygdala using multi-contrast MR imaging. Neuroimage 58:549–559.

Jesmanowicz A, Bandettini PA, Hyde JS (1998): Single-shot half k-space high-resolution gradient-recalled EPI for fMRI at 3 tesla. Magn Reson Imaging 40:754–762.

Kanai R, Bahrami B, Roylance R, Rees G (2011): Online social network size is reflected in human brain structure. Proc R Soc B 279:1327–1334.

Kerchner GA, Hess CP, Hammond-Rosenbluth KE, Xu D, Rabinovici GD, Kelley DAC, Vigneron DB, Nelson SJ, Miller BL (2010): Hippocampal CA1 apical neuropil atrophy in mild Alzheimer disease visualized with 7-T MRI. Neurology 75: 1381–1387.

Kim N, Kim HJ, Hwang J, Yoon SJ, Cho HB, Renshaw PF, Lyoo IK, Kim JE (2011): Amygdalar shape analysis method using surface contour aligning, spherical mapping, and probabilistic subregional segmentation. Neurosci Lett 488:65–69.

Konrad C, Ukas T, Nebel C, Arolt V, Toga AW, Narr KL (2009): Defining the human hippocampus in cerebral magnetic

resonance images—An overview of current segmentation protocols. Neuroimage 47:1185–1195.
LeDoux J (2007): The amygdala. Curr Biol 17:868–874.
Lee J, Fukunaga M, Duyn JH (2011): Improving contrast to noise ratio of resonance frequency contrast images (phase images) using balanced steady-state free precession. Neuroimage 54: 2779–2788.
Luders E, Thompson PM, Narr KL, Toga AW, Jancke L, Gaser C (2006): A curvature-based approach to estimate local gyrification on the cortical surface. Neuroimage 29:1224–1230.
Lüsebrink F, Wollrab A, Speck O (2012): Cortical thickness determination of the human brain using high resolution 3T and 7T MRI data. Neuroimage 70:122–131.
Madan N, Grant PE (2009): New directions in clinical imaging of cortical dysplasias. Epilepsia 50 (Suppl 9): 9–18.
Mai JK, Paxinos G, Voss T (2007): Atlas of the Human Brain. Academic Press, San Diego, California, USA.
Malykhin NV, Bouchard TP, Ogilvie CJ, Coupland NJ, Seres P, Camicioli R (2007): Three-dimensional volumetric analysis and reconstruction of amygdala and hippocampal head, body and tail. Psychiatry Res 155:155–165.
Menon RS, Goodyear BG (1999): Submillimeter functional localization in human striate cortex using BOLD contrast at 4 Tesla: Implications for the vascular point-spread function. Magn Reson Med 41:230–235.
Morey RA, Petty CM, Xu Y, Hayes JP, Wagner HR II, Lewis DV, LaBar KS, Styner M, McCarthy G (2009): A comparison of automated segmentation and manual tracing for quantifying hippocampal and amygdala volumes. Neuroimage 45:855–866.
Murty VP, Ritchey M, Adcock RA, LaBar KS (2011): Reprint of: fMRI studies of successful emotional memory encoding: a quantitative meta-analysis. Neuropsychologia 49:695–705.
Polimeni JR, Fischl B, Greve DN, Wald LL (2010): Laminar analysis of 7T BOLD using an imposed spatial activation pattern in human V1. Neuroimage 52:1334–1346.
Prudent V, Kumar A, Liu S, Wiggins G, Malaspina D, Gonen O (2010): Human hippocampal subfields in young adults at 7.0 T: Feasibility of imaging. Radiology 254:900–906.
Pruessner JC, Li LM, Serles W, Pruessner M, Collins DL, Kabani N, Lupien S, Evans AC (2000): Volumetry of hippocampus and amygdala with high-resolution MRI and three-dimensional analysis software: Minimizing the discrepancies between laboratories. Cereb Cortex 10:433–442.
Richardson MP, Strange BA, Dolan RJ (2004): Encoding of emotional memories depends on amygdala and hippocampus and their interactions. Nat Neurosci 7:278–285.
Rilling JK, Scholz J, Preuss TM, Glasser MF, Errangi BK, Behrens TE (2011): Differences between chimpanzees and bonobos in neural systems supporting social cognition. Soc Cogn Affect Neurosci 7:369–379.
Saygin ZM, Osher DE, Augustinack J, Fischl B, Gabrieli JDE (2011): Connectivity-based segmentation of human amygdala nuclei using probabilistic tractography. Neuroimage 56:1353–1361.
Schumann CM, Hamstra J, Goodlin-Jones BL, Lotspeich LJ, Kwon H, Buonocore MH, Lammers CR, Reiss AL, Amaral DG (2004): The amygdala is enlarged in children but not adolescents with autism; the hippocampus is enlarged at all ages. J Neurosci 24: 6392–6401.
Solano-Castiella E, Schäfer A, Reimer E, Türke E, Pröger T, Lohmann G, Trampel R, Turner R (2011): Parcellation of human amygdala in vivo using ultra high field structural MRI. Neuroimage 58:741–748.
Squire LR, Zola-Morgan S (1991): The medial temporal lobe memory system. Science 253:1380–1386.
Swanson LW, Petrovich GD (1998): What is the amygdala? Trends Neurosci 21:323–331.
Thomas BP, Welch EB, Niederhauser BD, Whetsell WO Jr, Anderson AW, Gore JC, Avison MJ, Creasy JL (2008): High-resolution 7T MRI of the human hippocampus in vivo. J Magn Reson Imaging 28:1266–1272.
Tsao J (2010): Ultrafast imaging: Principles, pitfalls, solutions, and applications. J Magn Reson Imaging 32:252–266.
Van de Moortele P-F, Auerbach EJ, Olman C, Yacoub E, Uğurbil K, Moeller S (2009): T1 weighted brain images at 7 Tesla unbiased for proton density, T2* contrast and RF coil receive B1 sensitivity with simultaneous vessel visualization. Neuroimage 46:432–446.
Vlachos I, Herry C, Lüthi A, Aertsen A, Kumar A (2011): Context-dependent encoding of fear and extinction memories in a large-scale network model of the basal amygdala. PLoS Comput Biol 7:e1001104.
Watson C, Andermann F, Gloor P, Jones-Gotman M, Peters T, Evans A, Olivier A, Melanson D, Leroux G (1992): Anatomic basis of amygdaloid and hippocampal volume measurement by magnetic resonance imaging. Neurology 42:1743–1750.
Yang S, Yang Z, Fischer K, Zhong K, Stadler J, Godenschweger F, Steiner J, Heinze HJ, Bernstein HG, Bogerts B, Mawrin C, Reutens DC, Speck O, Walter M, (2013): Integration of ultra-high field MRI and histology for connectome based research of brain disorders. Front Neuroanat 7(31).
Yushkevich PA, Avants BB, Pluta J, Das S, Minkoff D, Mechanic-Hamilton D, Glynn S, Pickup S, Liu W, Gee JC, Grossman M, Detre JA (2009): A high-resolution computational atlas of the human hippocampus from postmortem magnetic resonance imaging at 9.4 T. Neuroimage 44:385–398.